THE JOURNAL OF PHYSICAL CHEMISTRY A

A JOURNAL OF THE AMERICAN CHEMICAL SOCIETY

July 23, 2026
Volume 130
Number 29
pubs.acs.org/JPCA

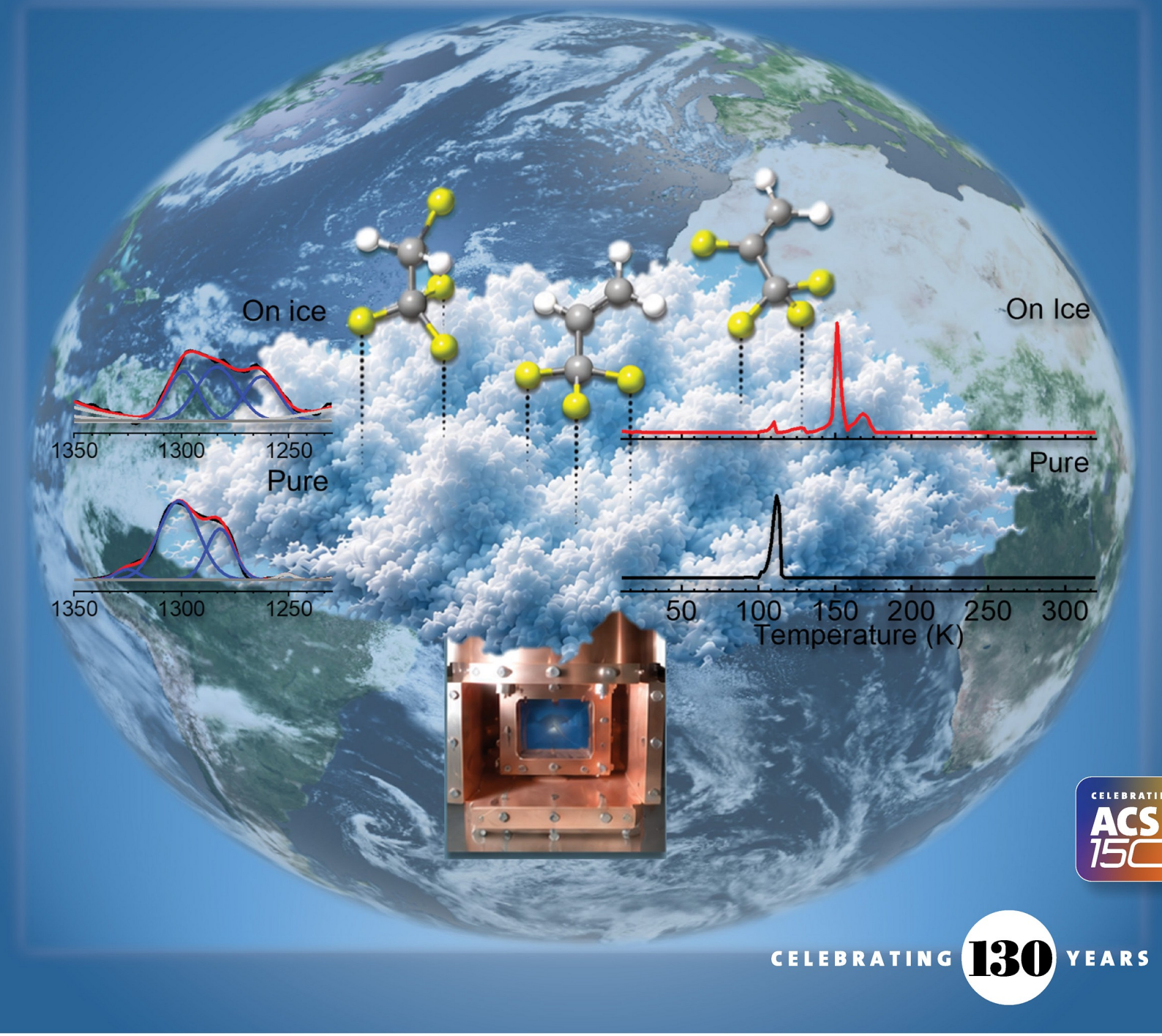

CELEBRATING 130 YEARS

ACS Publications
Most Trusted. Most Cited. Most Read.

www.acs.org

THE JOURNAL OF PHYSICAL CHEMISTRY A
A JOURNAL OF THE AMERICAN CHEMICAL SOCIETY

pubs.acs.org/JPCA Article

Determining Binding Energies of Key Fluorinated Refrigerants 1,1,1,2-Tetrafluoroethane, 2,3,3,3-Tetrafluoropropene, and 3,3,3-Trifluoropropene

Koushik Mondal, Mason McAnally, Nils Melbourne, Andrew M. Turner, Alexandre Bergantini, Rui Sun,* and Ralf I. Kaiser*

Cite This: J. Phys. Chem. A 2026, 130, 5707−5717 Read Online

ACCESS | Metrics & More | Article Recommendations | Supporting Information

ABSTRACT: Ice surfaces in the upper troposphere and polar regions act as chemically active interfaces that regulate the uptake and fate of trace gases; however, the interactions of fluorinated refrigerants with amorphous solid water (ASW) have remained poorly constrained. Here, we combine temperature-programmed desorption (TPD), infrared (IR) spectroscopy, and density functional theory (DFT) to investigate the adsorption of 1,1,1,2-tetrafluoroethane (HFC-134a; CF_3CH_2F), 2,3,3,3-tetrafluoropropene (R1234yf; $CF_3CF{=}CH_2$), and 3,3,3-trifluoropropene (R1243zf; $CF_3CH{=}CH_2$) on porous ASW. TPD profiles reveal a pronounced shift in the primary desorption feature from 95−105 K (pure films) to 140−152 K on ASW, indicating enhanced binding. Desorption energies are (51 ± 4), (48 ± 3), and (45 ± 6) kJ mol^{-1}, respectively, with an additional codesorption feature at 155−170 K evidencing partial trapping within the ice matrix. IR spectra exhibit red shifts of 11−21 cm^{-1} in the 1000−1500 cm^{-1} C−F stretching region, consistent with hydrogen bonding with the surface water network and long-range dipole interaction. DFT calculations reproduce these shifts and identify adsorption geometries governed by fluorine−OH interactions. These results demonstrate that fluorinated refrigerants can be transiently sequestered on ice, with implications for their atmospheric transport and reactivity.

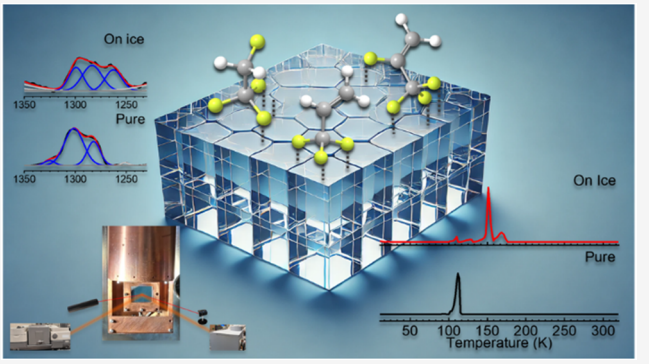

1. INTRODUCTION

Ice surfaces are chemically active interfaces that strongly influence the atmospheric fate of trace gases in cold environments such as the polar stratosphere, upper troposphere, and wintertime boundary layers. Heterogeneous adsorption on ice controls gas−surface partitioning, exposure to photochemistry, and access to multiphase reaction pathways central to halogen activation and ozone depletion. Seminal laboratory, field, and modeling studies have established that ice and snow are not inert substrates but actively mediate chemical transformations in polar stratospheric clouds, cirrus ice, and snowpacks.[1−4]

This is of particular importance to hydrofluorocarbons (HFCs) and hydrofluoroolefins (HFOs), widely used as refrigerants and foam-blowing agents. Although these compounds were developed to suppress halogen-driven ozone loss, chemistry−climate model simulations demonstrate that their strong radiative forcing alters stratospheric temperatures and circulation, indirectly enhancing ozone-destroying catalytic cycles and leading to non-negligible ozone depletion potentials.[5,6] These findings place HFCs and HFOs within the broader framework of cryosphere−atmosphere coupling, where heterogeneous interactions may influence both climate and chemistry.

Whereas gas-phase degradation of refrigerants is anticipated by relatively high activation barriers of tens of kJ mol^{-1} that strongly suppress reactivity under cold atmospheric conditions,[7] adsorption on ice surfaces stabilizes reactants through hydrogen bonding and orientational confinement, effectively lowering the energetic cost of interaction and enabling condensed-phase chemistry; this contrast motivates the present study which combines temperature-programmed desorption (TPD) and infrared (IR) spectroscopy to quantitatively investigate binding energies and adsorption-induced vibrational shifts of these species. The results are further interpreted further interpreted using density functional theory (DFT) calculations.[7,8]

Received: April 9, 2026
Revised: June 25, 2026
Accepted: June 26, 2026
Published: July 2, 2026

https://doi.org/10.1021/acs.jpca.6c02265
J. Phys. Chem. A 2026, 130, 5707−5717

Table 1. Compilation of Molecular Structures, Formulae, Common Names, and Abbreviations Used in This Publication

Structure	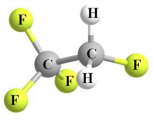	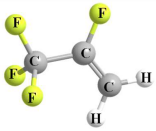	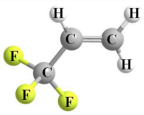
Molecular formula	CF_3CH_2F	CF_3CFCH_2	CF_3CHCH_2
IUPAC name	1,1,1,2–tetrafluoroethane	2,3,3,3–tetrafluoropropene	3,3,3–trifluoropropene
Common name	HFC134a	R-1234yf	R-1243zf
Name used here	R-I	R-II	R-III

At the molecular level, ice surface reactivity is controlled by dangling OH (d_{OH}) groups, formed by subcoordinated water molecules at amorphous ice surfaces, pores, and grain boundaries. Early infrared studies identified sharp free−OH stretching features near 3720 cm^{-1} and 3694 cm^{-1}, assigned to two- and three-coordinated surface water molecules, respectively, in contrast to the broad bulk OH band centered at 3200−3300 cm^{-1}.[9−11] A substantial body of experimental and theoretical work has demonstrated that fluorinated and halogenated molecules interact with ice primarily through directional hydrogen bonding at dangling OH sites. Infrared spectroscopy, helium atom scattering, and molecular simulation studies have reported binding energies of 15−40 kJ mol^{-1} for fluorinated methanes and up to 40−50 kJ mol^{-1} for fluorinated alcohols and oxygenated species adsorbed on solid water ices.[12−16] These interaction strengths are sufficient to promote temporary sequestration on ice particles at tropospheric temperatures and to modify surface vibrational dynamics.

Despite this progress, prior studies have largely focused on simple fluorinated methane derivatives (CH_nF_{4-n}) or oxygenated halocarbons, leaving a critical gap for modern long chain fluorinated refrigerants, which are now dominating industrial applications. In particular, 1,1,1,2-tetrafluoroethane (CF_3CH_2F; HFC-134a) and the low-global-warming-potential HFOs 2,3,3,3-tetrafluoropropene ($CF_3CF{=}CH_2$; R1234yf) and 3,3,3-trifluoropropene ($CF_3CH{=}CH_2$; R1243zf) have not yet been systematically characterized at the molecular level on ice surfaces. In addition, the oxidation of refrigerants yields trifluoroacetic acid (TFA), a persistent atmospheric end product whose formation in the upper troposphere and subsequent transport and scavenging under cold conditions highlight the potential importance of ice-mediated interactions in controlling the fate of fluorinated species.[17−19] Quantitative data on their binding energies, adsorption geometries, and vibrational shifts are lacking, limiting our ability to assess their heterogeneous uptake, residence times on ice particles, and potential role in ice-mediated atmospheric chemistry.

In this work, we address this gap through a combined experimental and theoretical investigation to determine the adsorption energetics and vibrational signatures of HFC-134a [1,1,1,2-tetrafluoroethane; CF_3CH_2F; (R-I)], R1234yf [2,3,3,3-tetrafluoropropene; $CF_3CF{=}CH_2$; (R-II)], and R1234zf [3,3,3-trifluoropropene; $CF_3CH{=}CH_2$; (R-III)] on ice (Table 1). By directly correlating experimentally observed binding energies and adsorption configurations, this study provides a molecular-level framework for understanding how modern refrigerants interact with ice surfaces, advancing the mechanistic basis required for improved representation of fluorinated greenhouse gases in cold-atmosphere chemistry.

2. EXPERIMENTAL AND COMPUTATIONAL

2.1. Experimental Section

All experiments were performed in a 304 stainless steel ultrahigh vacuum (UHV) chamber.[20−25] The chamber was evacuated to a base pressure of 5 × 10^{-11} Torr using an oil-free pumping system consisting of a magnetically levitated turbomolecular pump (Osaka, TG1121 MCA) in series with a second turbomolecular pump (Osaka, TG420 MCAC), backed by an oil-free scroll pump (Edwards XDS35i). A polycrystalline silver substrate mounted at the center of the chamber served as the deposition target. The substrate was attached to a cold head (CTI Cryodyne 1020C) cooled by a two-stage closed-cycle helium refrigerator (Cryodyne 9600 compressor), enabling temperature control down to 10.0 ± 0.5 K. Temperature was monitored using a calibrated silicon diode sensor (DT-670, Lakeshore Cryotronics) and regulated by a Lakeshore 336 temperature controller. The cold head assembly was mounted on a differentially pumped, rotatable flange, allowing angular adjustment within the experimental plane. Gas deposition was performed through a precision leak valve connected to a glass capillary array with 10 μm pore diameter, ensuring controlled and reproducible dosing onto the substrate surface.

2.2. Ice Preparation and Deposition Protocols

To determine binding energies on the silver target, neat refrigerant ices were prepared by depositing high-purity refrigerant gases 1,1,1,2-Tetrafluoroethane (HFC 134a, R-I, 99.9%, Chemours), 2,3,3,3-Tetrafluoropropene (R 1234yf, R-II, 99.9%, Chemours), and 3,3,3-Trifluoropropene (R 1243zf, R-III, 99.9%, Pfaltz & Bauer) onto the silver substrate held at 10 K at a constant pressure of 5 × 10^{-7} Torr during deposition. The binding energies of these refrigerants R-I, R-II and R-III were also determined on amorphous solid water (ASW) through the deposition of 20−50 nm of refrigerants at 5 × 10^{-9} Torr onto a 500 ± 10 nm film of 99.99% water ice at 10 K. A set of co-deposition experiments was also performed to determine binding energies of the refrigerants mixed at levels of 1% within ASW.

2.3. Infrared Spectroscopic Characterization

Ice film thicknesses were controlled via deposition time and monitored *in situ* using laser interferometry.[20,25,26] All deposited ices were characterized using absorption−reflection−absorption infrared spectroscopy over the spectral range 500−5000 cm^{-1}. Infrared light from an FTIR spectrometer operated in absorption−reflection mode (Nicolet 6700, Thermo Scientific) was directed at an angle of 75° perpendicular to the silver substrate through a 35 mm zinc selenide (ZnSe) window mounted on a CF flange. The reflected beam was recollimated and focused onto a liquid nitrogen-cooled mercury cadmium telluride (MCT-B) detector using second-stage transfer optics. For a quantitative analysis and initial column density determination, spectra were collected over 30 min at 4 cm^{-1} resolution, averaging 3,360 scans per spectrum to optimize signal-to-noise ratio. During TPD experiments, spectra were recorded every 2 min by averaging 224 scans. Column densities (N, molecules cm^{-2}) were calculated from the integrated absorbance values using previously measured band strengths for the strongest C−F stretching modes of each refrigerant.[25] The average column density (N) of R-I,

https://doi.org/10.1021/acs.jpca.6c02265
J. Phys. Chem. A 2026, 130, 5707−5717

R-II and R-III (6.52 ± 0.65) × 10^{18} molecules cm^{-2} (4.25 ± 0.5) × 10^{18} molecules cm^{-2} and (3.85 ± 0.42) × 10^{18} molecules cm^{-2}, respectively, were utilized to determine binding energies of the pure refrigerants from the silver surface. R-I, R-II, and R-III column densities (N) were varied in the range (4.5−8.8) ± 0.5 × 10^{16} molecules cm^{-2} in case of layered and co-deposition experiments on ASW.

2.4. Temperature-Programmed Desorption (TPD) Measurements

Temperature-programmed desorption (TPD) is a valuable method to determine binding energies where the deposited ices are heated at a certain heating rate, followed by subsequent determination of the concentration of sublimated species through calibrated mass spectrometry.[27−30] Here, the temperature of the deposited ices was increased from 10 to 320 K at a rate of 1 K min^{-1} exploiting the Lakeshore 336 temperature controller linked to a calibrated silicon diode sensor (DT-670, Lakeshore Cryotronics). During TPD experiments, ion currents (A) corresponding to selected mass fragments were recorded as a function of temperature using a quadrupole mass spectrometer (QMS; QME 422, Pfeiffer Vacuum) with an emission current of 2 mA and electron energy of 100 eV. All refrigerants investigated in this study contain a trifluoromethyl (CF_3) functional group; the fragment ion corresponding to CF_3^+ (m/z = 69) represents one of the dominant signals in their mass spectra as evident from the temperature-programmed desorption (TPD) profiles of the refrigerants (Figure S1). For a quantitative analysis, the refrigerant concentrations during TPD were monitored through the calibrated mass signal corresponding to m/z = 69 (CF_3^+), while calibrated m/z = 18 (H_2O^+) ion currents were used to determine water concentration during TPD. The raw TPD traces, initially represented as ion current versus temperature, were converted to desorption flux (ϕ, ML K^{-1}; ML = mono layers) through calibration of the quadrupole mass spectrometer (QMS) signal with spectroscopically determined column densities (N in molecules cm^{-2}), followed by conversion of column densities to surface coverages (θ, ML; ML = mono layers).[28,30] To calibrate the ion current (in A) during TPD of a particular species into absolute surface concentrations or column density (N in molecules cm^{-2}), the overall integrated area of the full TPD trace of any major mass fragment (m/z = 69; CF_3^+) was considered to be spectroscopically determined initial column density (N) of that species. For conventional surface science comparison, column densities were further converted into surface coverage (θ) represented in terms of monolayer (ML) units with 1 ML = 10^{15} molecules cm^{-2}.

2.5. Kinetic Framework and Evaluation of Binding Energies from TPD

The binding energy of an adsorbate to a surface is a key physicochemical parameter that governs surface residence times, diffusion kinetics, and gas−surface partitioning under low-temperature conditions. Experimentally, binding energies are most commonly derived from temperature-programmed desorption (TPD) measurements. The combined use of TPD and spectroscopic characterization provides a robust experimental framework for extracting physically meaningful binding energies from heterogeneous ice surfaces. TPD analysis is rooted in the Polanyi−Wigner formalism, in which the desorption rate is expressed as a function of column density (N), temperature (T), reaction order (n), and desorption energy (E_{des} equivalent to binding energy E_b). The classical treatments by Redhead and King established the theoretical basis for extracting binding energies (E_b) from peak desorption temperatures under controlled heating rates, assuming well-defined desorption orders (n) and negligible readsorption.[27,28,30−33] For an adsorbate with column density N on a surface, the desorption rate r_{des} is expressed as

$$r_{des} = -\frac{dN}{dt} = \nu_n N^n \exp\left(-\frac{E_b}{k_B T}\right) \quad (1)$$

where n is the order of desorption, ν_n is the pre-exponential factor, E_b is the binding energy, T is the temperature in Kelvin (K), k_B and is the Boltzmann constant. For a linear temperature ramp ($\beta = dT/dt$) (K s^{-1}) during TPD, the desorption rate can be transformed in terms of desorption flux (ϕ) and surface coverage at any temperature (θ(T)) as[28]

$$\phi = -\frac{d\theta}{dT} = \frac{\nu_n}{\beta}\theta(T)^n \exp\left(-\frac{E_b}{k_B T}\right) \quad (2)$$

In the present experiments, the heating rate β was maintained constant at 0.016 K s^{-1} (1 K min^{-1}) throughout all TPD measurements. The desorption order n typically assumes values of 0 or 1, depending on the nature of the surface and the adsorbate−adsorbate interactions. Desorption from multilayer molecular solids commonly follows zeroth-order kinetics, whereas desorption from heterogeneous surfaces such as amorphous water (ASW) ice often follows first-order kinetics. For zeroth-order desorption, eq 2 can be rearranged into the linear form

$$\ln(\phi) = \ln\left(\frac{\nu_0}{\beta}\right) - \frac{E_b}{k_B T} \quad (3)$$

Thus, a plot of $\ln(\phi)$ versus $1/T$ yields a straight line whose slope and intercept correspond to E_b and ν_0, respectively. The linearity of this relationship provides experimental confirmation of zeroth-order desorption behavior.[28,29]

The temperature-programmed desorption (TPD) fluxes corresponding to desorption from heterogeneous surfaces, such as amorphous solid water (ASW), are analyzed using eq 2 with first-order desorption kinetics (n = 1) and performing nonlinear exponential fitting implemented in Python. The conventional approach for determining the optimized binding energy involves generating a series of simulated TPD flux profiles through systematic variation of the binding energy (E_b) over a range consistent with the experimentally determined fractional surface coverage change, $\theta(T)/\theta_0$, during a sublimation event. The simulated flux profiles are subsequently compared with the experimental data using least-squares analysis, quantified in terms of the coefficient of determination (R^2), to identify the set of parameters that maximizes the goodness of fit.

However, the pre-exponential factor (ν_n) in eq 2 plays a significant role in determining the quality of the fit, as it depends on the degree of surface heterogeneity and the specific nature of the sublimation process. Consequently, applying the same nonlinear fitting procedure while allowing the pre-exponential factor to vary produces a family of fitted curves. These fits are likewise evaluated using least-squares analysis to determine the optimal parameter set. In practice, the pre-exponential factors typically were varied by two to 3 orders of magnitude relative to the zero-order pre-exponential factor (ν_0), to corelate variations in surface heterogeneity and the mechanism of the sublimation event.

2.6. Computational Methodologies

The equilibrium geometries of the isolated refrigerants, as well as configurations corresponding to adsorption on the surface of water clusters and incorporation within the cluster matrix, were optimized using density functional theory (DFT) as implemented in the *NWChem* program package. All calculations were performed at the B3LYP-D3/6−31+G* level of theory at 0 K.[34,35] The hybrid B3LYP functional provides a well-established compromise between computational efficiency and accuracy for predicting vibrational properties of halogenated hydrocarbons, while the inclusion of Grimme's D3 dispersion correction accounts for long-range intermolecular interactions that are otherwise inadequately described at the B3LYP level.[36] Geometry relaxations of full ice encapsulation systems were performed with all atoms active, while for ice surface systems, only the atoms of the refrigerant and top layer of ice were allowed to relax. Following geometry optimization, harmonic vibrational frequencies were obtained from analytic second derivatives of the energy with respect to nuclear displacements. The calculated frequencies for configurations in which refrigerants reside on the surface of the water cluster were directly compared with experimental results obtained under layered deposition conditions, whereas frequencies correspond-

https://doi.org/10.1021/acs.jpca.6c02265
J. Phys. Chem. A 2026, 130, 5707−5717

ing to refrigerants embedded within the cluster were correlated with co-deposition experiments, thereby enabling a consistent structural interpretation of the spectroscopic observations. Rather than employing a uniform scaling factor as recommended by the NIST Computational Chemistry Comparison and Benchmark Database (CCCBD) for B3LYP/6−31+G* calculations, a system-specific calibration was adopted to account for residual errors arising from the harmonic approximation and functional/basis set limitations deficiencies. Specifically, scaling factors were derived from the slopes of linear regressions between experimentally measured vibrational frequencies at 10 K and the corresponding unscaled theoretical frequencies computed at 0 K (Figure S2a−c). The resulting scaling factors were determined to be 0.983 ± 0.001, 1.004 ± 0.001, and 0.981 ± 0.001 for R-I, R-II, and R-III, respectively; these factors were subsequently applied to all calculated frequencies to facilitate direct comparison with experimental spectra.

3. RESULTS AND DISCUSSION

3.1. TPD Studies

The calibrated TPD profiles in terms of desorption flux (ϕ, ML K^{-1}) for refrigerants R-I, R-II, and R-III are presented in Figure 1(a−c). In each figure, the bottom trace (black trace) corresponds to the TPD profile for the desorption of pure refrigerant from the silver substrate, while the center (red trace) and top trace (blue trace) represent the layered deposition on water ice, and co-deposition with water vapor, respectively. For the pure refrigerants, the TPD profiles exhibit a single sublimation event (S_1) corresponding to sublimation of the molecular solid from the silver substrate, while layered and co-deposition on ASW exhibits two more sublimation events at elevated temperature, denoted by S_2 and S_3. Depending on the molecular identity of the refrigerant, the temperature of the S_1 sublimation event varies in pure-deposition experiments. The S_1 sublimation temperatures were determined to be (107 ± 2) K for R-I, (95 ± 2) K for R-II, and (97 ± 2) K for R-III. In contrast, the S_1 sublimation event exhibits different behavior when the refrigerants are deposited as a layer on amorphous solid water (ASW). In the TPD profiles of all refrigerants under multilayer coverage, an additional sublimation feature is observed between the S_1 and S_2 events. This intermediate desorption peak is attributed to the sublimation of a second population of refrigerant molecules that are not directly bound to the ASW surface but instead reside in an overlayer above the adsorbed interfacial molecules.

The S_2 peak, occurring between 140 and 152 K often termed as "molecular volcano" corresponds to desorption from the pores that collapse during the structural reorganization of ASW while the S_3 peak, observed between 155 and 170 K, represents codesorption of trapped molecules with the sublimation of water ice. The ratio of the desorption fluxes associated with the S_2 and S_3 sublimation events differs significantly between the co-deposition and layered-deposition experiments for all refrigerants. In particular, the higher refrigerant flux observed during the S_3 sublimation event in the co-deposition experiments, relative to the layered-deposition experiments, indicates a greater abundance of refrigerant molecules trapped within the ASW matrix and subsequently codesorbing with water. This behavior is consistent with the expected enhanced trapping of refrigerants during co-deposition.

3.2. Binding Energies

To determine the binding energies of the pure refrigerants, the TPD traces corresponding to the sublimation peak S_1 were

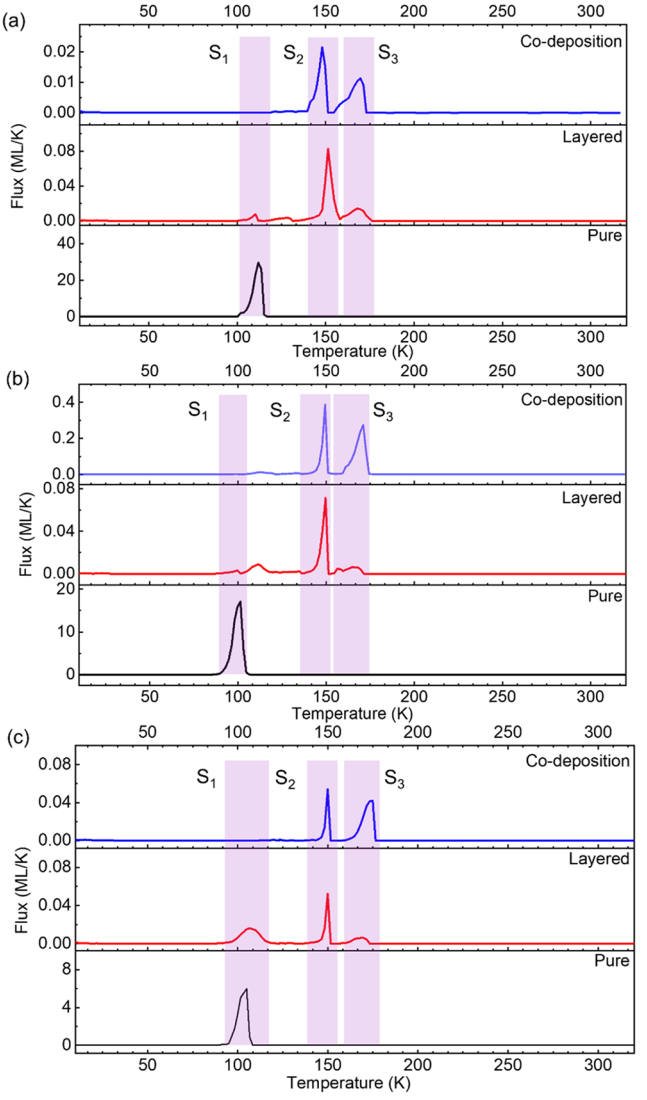

Figure 1. Temperature-programmed desorption (TPD) profiles of the investigated refrigerants: neat refrigerant (black, bottom), layered deposition on amorphous solid water (ASW, red, middle), and co-deposition with ASW (blue, top). (a) R-I, (b) R-II, and (c) R-III. Neat films exhibit a single desorption event (S_1) from the silver substrate, whereas additional higher-temperature events (S_2 and S_3) emerge for ASW systems indicating enhanced binding and partial trapping of refrigerant molecules within the amorphous ice matrix.

analyzed using the zeroth-order kinetic treatment described above. The ln(ϕ) vs 1/T plots for R-I, R-II, and R-III are presented in Figure 2(a−c). The excellent linearity of these plots confirms that the sublimation of the pure refrigerants follows zeroth-order desorption kinetics. The evaluated binding energies (E_b) through the zeroth order kinetic treatment for R-I, R-II and R-III were (34 ± 1) kJ mol^{-1}, (30 ± 1) kJ mol^{-1} and (29 ± 1) kJ mol^{-1} respectively. While the corresponding pre-exponential factors were determined to be 5.73 × 10^{15} ML s^{-1} (R-I), 2.78 × 10^{15} ML s^{-1} (R-II) and 1.60 × 10^{14} ML s^{-1} (R-III).

The binding energies of refrigerants on amorphous solid water (ASW) considers analysis of TPD traces obtained from both the layered and co-deposition experiments. For both the experiments the binding energies associated with S_2 represent the interaction strength between refrigerants and ASW

https://doi.org/10.1021/acs.jpca.6c02265
J. Phys. Chem. A 2026, 130, 5707−5717

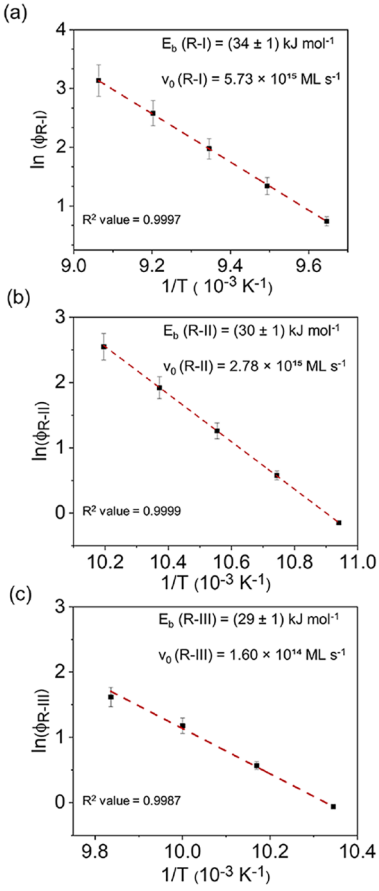

Figure 2. Arrhenius analysis of desorption kinetics for pure refrigerants. Plots of $\ln(\phi)$ versus $1/T$ corresponding to the primary desorption event (S1) are shown for (a) R-I, (b) R-II, and (c) R-III. Data were analyzed using a zero-order kinetic model, from which pre-exponential factors (ν_0) were obtained from the intercept ($\ln(\nu_0/\beta)$) and binding energies (E_b) from the slope ($-E_b/k_b$).

surfaces, while S_3 provides insight into molecule−ice interactions within mixed ice matrices. The desorption fluxes associated with S_2 and S_3 were analyzed using nonlinear exponential fitting of eq 2, implemented through the SciPy optimization routine (scipy.optimize.curve_fit).[28] Since both fractional surface coverage ($\theta(T)/\theta_0$) and binding energy (E_b) vary during the desorption process, the fitting procedure constrained θ within the experimentally measured range obtained from integrated TPD signals. The pre-exponential factor was initially fixed to the value determined for pure refrigerant desorption and subsequently varied within 2 to 3 orders of magnitude to optimize the goodness of fit. The fitting procedure generated families of possible solutions, represented as gray regions in Figures 3, 4, and 5, while the optimal solution corresponding to the highest R^2 value is indicated by red markers. The kinetic fitting procedure of the best fit plots of all the sets in terms of simultaneous variation of fractional surface coverage and binding energy (E_b) along with least-square analysis (in terms of R^2 value) are provided in Figures S3−S5.

The optimized binding energies of R-I, R-II and R-III through this analysis for the S_2 desorption event were determined to be (51 ± 4) kJ mol^{-1}, (48 ± 3) kJ mol^{-1} and (45 ± 6) kJ mol^{-1} for layered deposition while in co-deposition binding energies of the same refrigerants corresponding to same desorption event were (51 ± 4) kJ mol^{-1}, (49 ± 7) kJ mol^{-1} and (46 ± 5) kJ mol^{-1}. Similarly, the binding energies of R-I, R-II and R-III corresponding to the S_3 codesorption event for layered deposition were determined to be (38 ± 7) kJ mol^{-1}, (47 ± 3) kJ mol^{-1} and (42 ± 2) kJ mol^{-1} while in co-deposition binding energies of the same refrigerants corresponding to same desorption event were (33 ± 5) kJ mol^{-1}, (45 ± 6) kJ mol^{-1} and (43 ± 2) kJ mol^{-1}. Similar binding energies obtained for all refrigerants at the S_2 and S_3 sublimation events in both deposition experiments suggest that the nature of the refrigerant−water interactions on the ASW surface and within the ice matrix is largely independent of the deposition method. This observation further implies that refrigerants deposited through the layered-deposition approach become incorporated into the ice matrix during the structural reorganization of amorphous solid water occurring near the S_2 sublimation event.

Furthermore, the refrigerant ices formed here on ASW are expected to fall within the multilayer adsorption regime, for which the binding energy is generally independent of the number of adsorbed layers. A recent study of the hydrogen sulfide (H_2S)-compact ASW system reported comparable binding energies for both submonolayer and multilayer H_2S adsorption on ASW, supporting this interpretation.[37] In the present work, however, the refrigerant coverage was not reduced to the submonolayer regime because such low coverages are beyond the detection limit of our ice-thickness measurement technique based on laser interferometry.

3.3. Vibrational Analysis

The combination of temperature-programmed desorption (TPD) and vibrational spectroscopy provides complementary insights into adsorption processes by constraining adsorption geometries, surface heterogeneity, and intermolecular interactions. Such combined approaches are particularly useful for probing weakly bound adsorbates on heterogeneous ice surfaces, where adsorption energetics are strongly influenced by the interplay between adhesive interactions (molecule−surface) and cohesive interactions (molecule−molecule). Current experimental and theoretical understanding of fluorinated methane derivatives ($CH_nF_{(4-n)}$) interacting with ice surfaces suggests that adsorption behavior is governed by this delicate balance between surface and intermolecular forces. Nonpolar species such as tetrafluoro methane (CF_4) and methane (CH_4) interact only weakly with the ice lattice and often behave as quasi-gas-phase species at the interface.[12−14,16] In contrast, partially fluorinated analogues such as trifluoromethane or fluoroform (CHF_3) and difluoromethane (CH_2F_2) exhibit stronger adsorption and frequently form ordered multilayer structures on ice. The adsorption orientation of these molecules is largely dictated by their hydrogen-bonding capability. For example, molecules such as CH_2F_2 and CHF_3 preferentially orient their fluorine atoms toward the ice surface, allowing them to accept protons from dangling O−H groups and a hydrogen-bonded network on the ice surface, thereby form stabilizing hydrogen bonds.[16] The infrared spectrum of water vapor deposited at 10 K reveals the presence of two characteristic dangling O−H stretching modes at 3720 cm^{-1} and 3694 cm^{-1}, corresponding to two- and three-coordinated surface OH groups.[9,38−40] The presence of these features confirms the formation of porous amorphous solid water (ASW), as shown in Figure S6. The way of deposition of water vapor changes morphology of the structure of the ice varying

https://doi.org/10.1021/acs.jpca.6c02265
J. Phys. Chem. A 2026, 130, 5707−5717

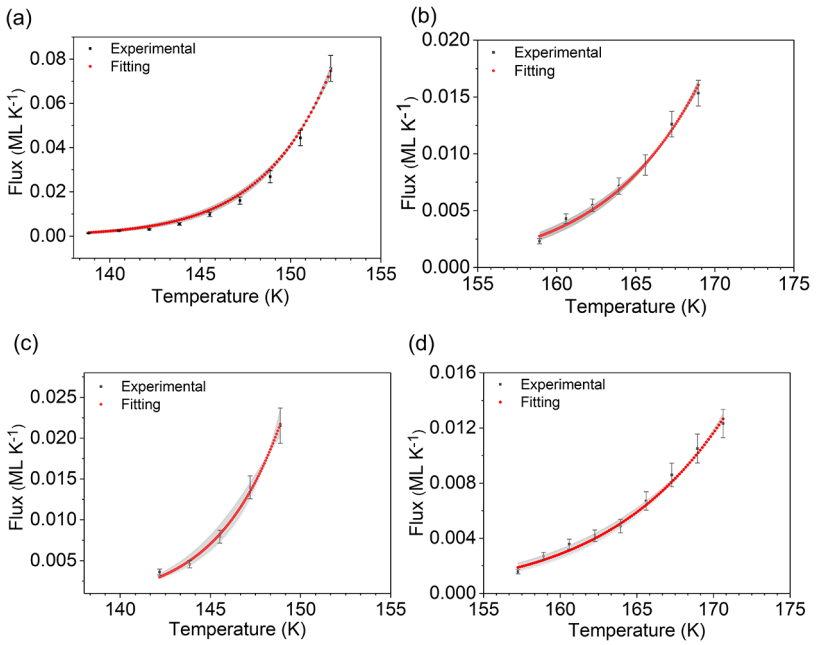

Figure 3. Determination of binding energies (E_b) for R-I on amorphous solid water using nonlinear least-squares fitting (SciPy) of TPD profiles based on eq 2. Results are shown for (a) S_2 (layered), (b) S_3 (layered), (c) S_2 (co-deposition), and (d) S_3 (co-deposition). Gray regions represent acceptable solutions across the experimentally constrained pre-exponential factor (ν_n) and surface coverage (θ), while the optimal fit with a maximum R^2 is indicated in red.

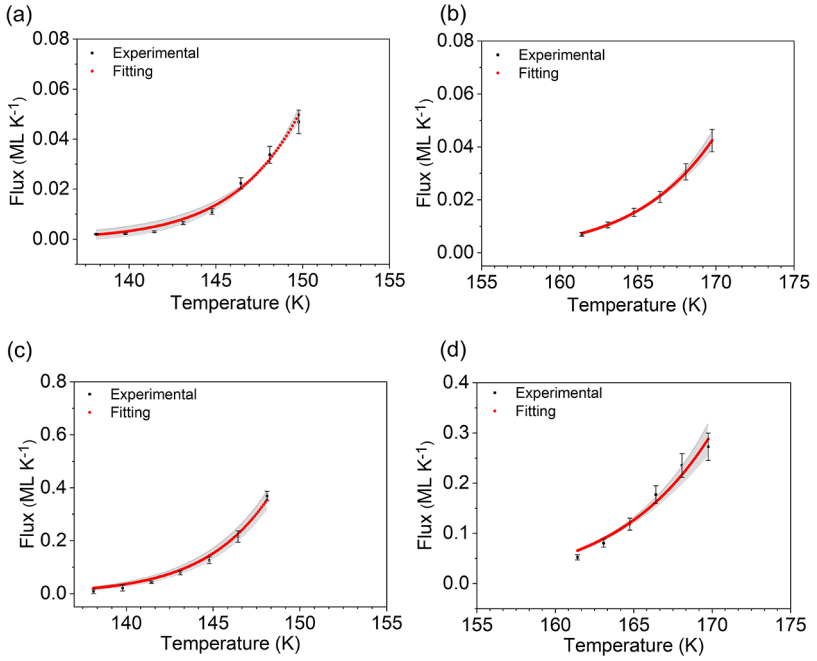

Figure 4. Determination of binding energies (E_b) for R-II on amorphous solid water using nonlinear least-squares fitting (SciPy) of TPD profiles based on eq 2. Results are shown for (a) S_2 (layered), (b) S_3 (layered), (c) S_2 (co-deposition), and (d) S_3 (co-deposition). Gray regions represent acceptable solutions across the experimentally constrained pre-exponential factor (ν_n) and surface coverage (θ), while the optimal fit with a maximum R^2 is indicated in red.

from like hexagonal (I_h) to cubic crystalline (I_c) to amorphous solid water ices (ASW). The formation of ASW after depositing water vapor in our experimental condition at 10 K also further confirmed through the presence of four broad absorption feature in the regions 3000−3600 cm^{-1}, 2000−2400 cm^{-1}, 1540−1780 cm^{-1} and 650−1000 cm^{-1} corresponding to stretching modes (symmetric (ν_1) and asymmetric (ν_3)), combination of libration modes (ν_L), bending mode (ν_2) and pure libration mode (ν_L) respectively detailed in Table S1 which is little bit different than that of infrared reflection absorption spectroscopy used for thin layer of ices.[40−45]

The refrigerants investigated in this study exhibit their strongest infrared absorption bands within the 1000−1500 cm^{-1} region, which primarily corresponds to vibrational modes associated with C−F bonds (Table S1). However, these

https://doi.org/10.1021/acs.jpca.6c02265
J. Phys. Chem. A 2026, 130, 5707−5717

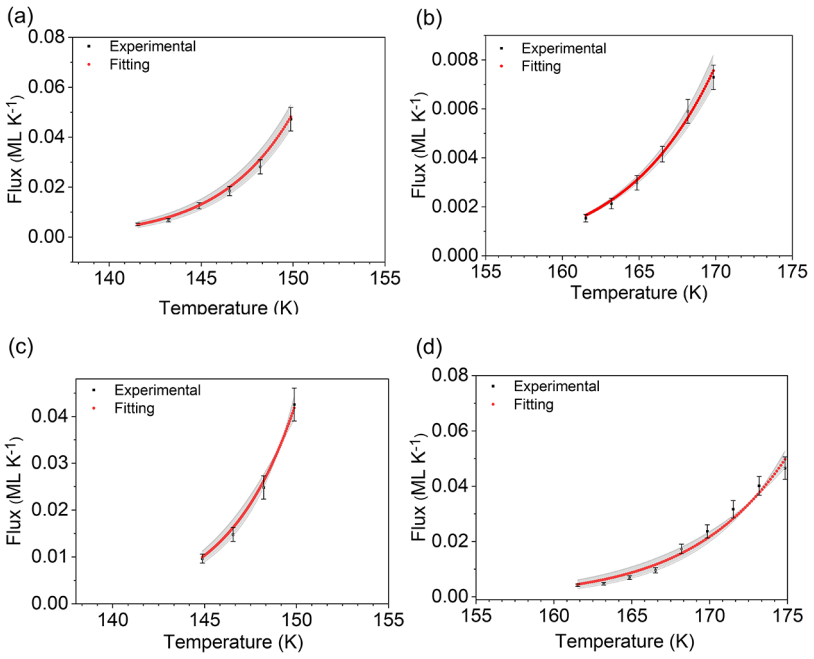

Figure 5. Determination of binding energies (E_b) for R-III on amorphous solid water using nonlinear least-squares fitting (SciPy) of TPD profiles based on eq 2. Results are shown for (a) S_2 (layered), (b) S_3 (layered), (c) S_2 (co-deposition), and (d) S_3 (co-deposition). Gray regions represent acceptable solutions across the experimentally constrained pre-exponential factor (ν_n) and surface coverage (θ), while the optimal fit with a maximum R^2 is indicated in red.

vibrational modes involve significant coupling between the C−F vibrations of the trifluoromethyl (CF_3) group and other internal molecular modes, as previously reported in the literature.[25] Consequently, adsorption-induced frequency shifts in this spectral region provide important insights into the nature of the molecule−ice interaction. Comparison of the vibrational spectra of R-I, R-II, and R-III deposited on ice surfaces with those of the corresponding pure molecular ices reveals measurable shifts in several vibrational frequencies for both layered and co-deposition experiments (Figure 6a−c and Table 2). For the pure refrigerant ices, the spectral features associated with the C−F vibrational modes in the 2000−500 cm^{-1} region undergo significant changes upon heating. The spectra recorded at temperatures near the S1 sublimation event differ markedly from those obtained at 10 K (Figure S7), indicating that the amorphous refrigerant ice undergoes structural reorganization and crystallization prior to sublimation.

These shifts indicate changes in the molecular environment and adsorption geometry upon interaction with the ice surface. For refrigerant R-I, the vibrational mode corresponding to CF_3 deformation coupled with CH_2 out-of-plane bending (ν_{13}) and CH_2 wagging (ν_4) exhibits a clear red shift from 1301 cm^{-1} to 1281 cm^{-1}. Similarly, the CF_3 deformation-CH_2 wagging (ν_4) mode shifts from 1283 cm^{-1} to 1260 cm^{-1}. These red shifts indicate that both the trifluoromethyl group and the CH_2 moiety participate in the interaction with the ice surface (Figure 6a).[25] In contrast, the vibrational modes associated with the C−F bond attached to the CH_2 group adjacent to the CF_3 unit show negligible frequency shifts, suggesting that this fluorine atom is not directly involved in surface binding and likely points away from the ice lattice (Figure 7a). The experimentally observed vibrational shifts are well supported by theoretical calculations. The most stable adsorption geometry predicted for layered deposition corresponds to a configuration in which the fluorine atom attached to the CH_2 group is oriented away from the ice lattice, while the CF_3 group interacts more directly with the surface. For refrigerant R-II, which contains a fluorine atom attached to an alkene moiety adjacent to the CF_3 group, the adsorption geometry differs significantly. In this case, both the fluorine atoms of the CF_3 group and the fluorine atom attached to the alkene unit interact with the ice lattice, leading to a configuration in which the molecule lies approximately coplanar with the ice surface (Figure 7b). Consistent with this geometry, the vibrational mode ν_{15} assigned to CF_3 deformation coupled with C−F stretching of the alkene and CH_2 rocking motion undergoes a red shift from 1172 cm^{-1} to 1155 cm^{-1}, in agreement with the theoretically predicted bound configuration.[25] In contrast, refrigerant R-III, whose vibrational spectrum is dominated by modes associated with the CF_3 functional group, exhibits a somewhat different adsorption behavior. The optimized adsorption geometry suggests that the molecule binds to the ice lattice at a tilted orientation, balancing interactions between the CF_3 fluorine atoms and the ice surface and weaker interactions involving the alkene C−H group and the ice lattice (Figure 7c). As a result, the vibrational shift associated with the CF_3 -coupled alkene vibrational mode (ν_{15}) is comparatively smaller than that observed for R-I and R-II. Overall, the combined experimental and theoretical vibrational analysis reveals that the adsorption geometries of the three refrigerants are governed by the distribution and accessibility of fluorine atoms capable of forming hydrogen-bond-like interactions with dangling OH groups on the ASW surface. These findings provide molecular-level insight into the adsorption configurations responsible for the binding energies extracted from the TPD experiments discussed above.

https://doi.org/10.1021/acs.jpca.6c02265
J. Phys. Chem. A 2026, 130, 5707−5717

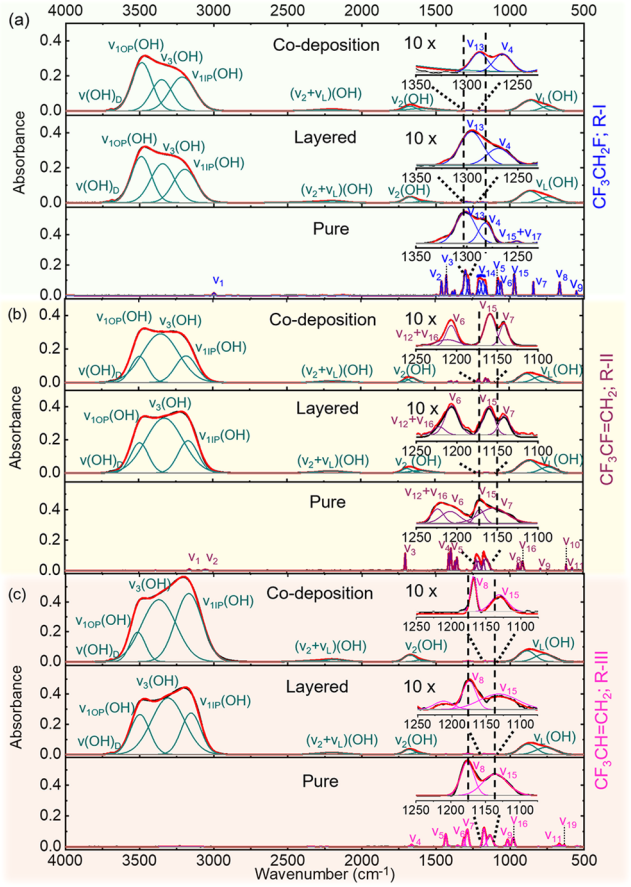

Figure 6. Infrared spectra in the C−F stretching region (1000−1500 cm^{-1}) for refrigerants: neat films (bottom), layered on ASW (middle), and co-deposited with ASW (top). (a) R-I, (b) R-II, and (c) R-III. Water features are highlighted in green, while refrigerant bands are indicated in blue (R-I), purple (R-II), and magenta (R-III). Observed frequency shifts in layered and co-deposition experiments with respect to pure films arise from water-refrigerant interactions. OP and IP denote out-of-plane and in-plane vibrational modes, respectively (Table S1).

4. SUMMARY AND CONCLUSION

Ice particles present in the upper troposphere and polar regions represent chemically active interfaces capable of controlling the uptake, transport, and heterogeneous processing of trace gases. In these cold environments, adsorption on amorphous solid water (ASW) can significantly alter the residence times and chemical fate of atmospheric species, particularly for compounds whose gas-phase reactions are kinetically inhibited at low temperatures. Despite the increasing atmospheric abundance of modern fluorinated refrigerants, quantitative data describing their adsorption energetics and binding geometries on ice surfaces remain scarce.

In this study, we investigate the low-temperature interactions of three technologically important refrigerants 1,1,1,2-tetrafluoroethane (HFC-134a; CF_3CH_2F), 2,3,3,3-tetrafluoropropene (R1234yf; $CF_3CF{=}CH_2$), and 3,3,3-trifluoropropene (R1243zf; $CF_3CH{=}CH_2$) with porous amorphous solid water using a combined temperature-programmed desorption (TPD), infrared spectroscopy, and density functional theory (DFT) approach under ultrahigh-vacuum conditions. Experiments performed at 10 K simulate cryogenic atmospheric environments where ice-mediated interactions become particularly important.

Partially fluorinated analogues such as trifluoromethane (fluoroform, CHF_3) and difluoromethane (CH_2F_2) are known to exhibit relatively strong adsorption on ice surfaces and to form multilayer adsorbate structures.[16] Therefore, investigating the binding energies associated with the multilayer adsorption of their trifluoromethyl-substituted analogue, R-I, as well as the olefinic analogues R-II and R-III, on amorphous solid water (ASW) is environmentally relevant. Shift in primary sublimation event from S_1 (95−105 K) to S_2 (140−152 K) in the TPD profile corresponding to refrigerants on ASW compared their pure deposition condition reveals existence of significantly strong binding to the ASW films. Analysis of these desorption events yields adsorption energies of (51 ± 4) kJ mol^{-1} for 1,1,1,2-tetrafluoroethane (HFC-134a; CF_3CH_2F), (48 ± 3) kJ mol^{-1} for 2,3,3,3-tetrafluoropropene (R1234yf; $CF_3CF{=}CH_2$) and (45 ± 6) kJ mol^{-1} for 3,3,3-trifluoropropene (R1243zf; $CF_3CH{=}CH_2$). Apart from the S_2 sublimation event existence of another co sublimation with water at S_3 (155−170 K) indicates partial trapping of refrigerant molecules within the ice matrix followed by codesorption during water sublimation. These results demonstrate that interactions between fluorinated refrigerants and ASW are sufficiently strong to enable temporary sequestration on atmospheric ice particles.

Infrared spectroscopic measurements further reveal adsorption-induced vibrational shifts within the 1000−1500 cm^{-1} C−F stretching region, confirming that the molecules interact with dangling OH groups present on porous ASW surfaces. For example, 1,1,1,2-Tetrafluoroethane (HFC 134a, R-I) exhibits

Table 2. Experimental Vibrational Frequencies (Exp) of the Investigated Refrigerants Recorded under Neat Deposition, Layered Deposition, and Co-Deposition Conditions on ASW Surfaces, together with the Corresponding Scaled Frequencies Obtained from Quantum Chemical Calculations[a,b]

	pure deposition		layered deposition		co-deposition		
refrigerant	exp	scaled	exp	scaled	Exp	scaled	mode assignment
R-I	1301	1289	1294	1287	1290	1286	ν_{13}; β(CC)/τ(CH_2 out-of-plane)
R-I	1283	1270	1266	1259	1260	1251	ν_4; ω(CH_2)/δ_s(CF_3)/σ(CC)
R-II	1172	1159	1159	1155	1157	1153	ν_{15}; δ_s(CF_3)/σ(C−F) /ρ(CH_2)
R-II	1155	1153	1140	1136	1138	1129	ν_7; σ_s(CF_3)/τ(CH_2)
R-III	1173	1141	1170	1142	1168	1166	ν_8; σ_{as}(CF_3)/ρ(HCH)/ δ(C=C−C) (in-plane)
R-III	1134	1120	1130	1132	1129	1130	ν_{15}; σ_{as}(CF_3)/τ(HCH) (in-plane)/δ(C=C−C) (out-of-plane)

[a]All frequencies are reported in cm^{-1}. The vibrational assignments correspond to the fundamental normal modes derived from theoretical analysis. [b]ν: Frequency; σ: Stretching; β: Bending; ρ: Rocking; δ: Deformation; ω: Wagging; τ: Twisting; s: symmetric; as asymmetric.

https://doi.org/10.1021/acs.jpca.6c02265
J. Phys. Chem. A 2026, 130, 5707−5717

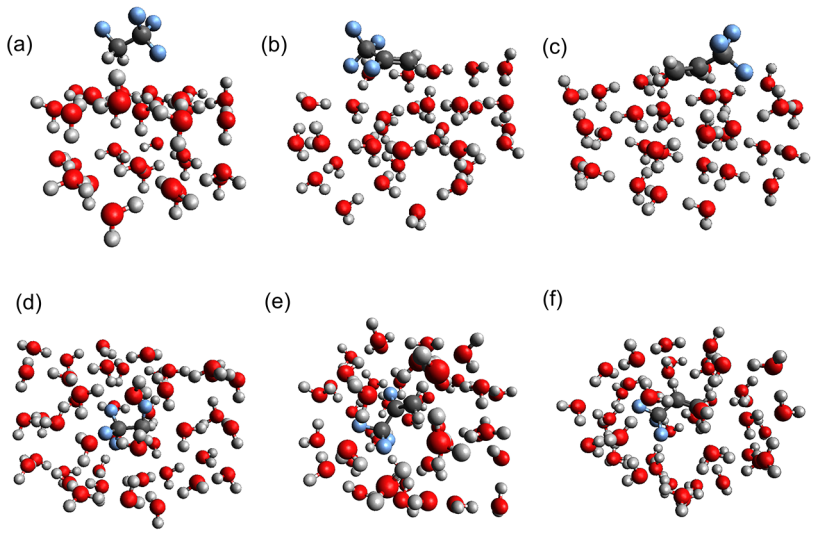

Figure 7. Computationally optimized adsorption geometries of refrigerants interacting with amorphous water clusters. Structures are shown for surface-bound configurations (top row) (a–c) and embedded configurations within the ice matrix (bottom row) (d–f): (a) R-I surface-bound, (b) R-II surface-bound, and (c) R-III surface-bound. (d) R-I within the ice matrix, (e) R-II within the ice matrix, and (f) R-III within the ice matrix. The geometries highlight preferential hydrogen-bonding interactions between fluorine atoms and surface OH groups. Optimized coordinates are provided in Table S2.

red shifts of 11–21 cm^{-1} in coupled CF_3–CH_2 vibrational modes, indicating cooperative interactions between the CF_3 functional group and surface hydroxyl sites while. The fluorine atom attached with alkene carbon in case of 2,3,3,3-tetrafluoropropene (R1234yf; $CF_3CF{=}CH_2$) interacts differently than that of 1,1,1,2-tetrafluoroethane (HFC-134a; CF_3CH_2F). Combined experimental and theoretical analysis suggests that adsorption geometries are controlled by the orientation and accessibility of fluorine atoms capable of accepting hydrogen bonds from surface OH groups.

These findings provide the first quantitative description of the adsorption energetics of modern refrigerants on amorphous water ice, revealing interaction strengths approaching 50 kJ mol^{-1}. Such binding energies imply that heterogeneous uptake on ice particles could influence the atmospheric transport and removal of these compounds and their oxidation products, including trifluoroacetic acid (TFA), in cold regions of the atmosphere. By establishing molecular-level adsorption parameters for key fluorinated refrigerants, this work addresses a critical knowledge gap and provides data needed to incorporate ice-mediated processes into atmospheric chemistry models.

■ ASSOCIATED CONTENT

Data Availability Statement

All the data are included in the manuscript and/or Supporting Information.

Supporting Information

The Supporting Information is available free of charge at https://pubs.acs.org/doi/10.1021/acs.jpca.6c02265.

Raw temperature-programmed desorption (TPD) profile of pure refrigerants (Figure S1); determination of calibration factor (Figure S2); correlation between fractional surface coverage (θ) and binding energy (E_b) obtained from nonlinear least-squares fitting (Figures S3–S5); infrared spectrum of amorphous solid water (ASW) (Figure S6); characteristic vibrational frequencies (cm^{-1}) of amorphous solid water (ASW) and pure refrigerant ices (R-I, R-II, and R-III) (Table S1); comparison of the infrared spectra of the pure refrigerants at 10 K and near the S1 sublimation event (Figure S7); coordinates of optimized refrigerants on ice surfaces and encapsulated within the ice matrix (Table S2) (PDF)

■ AUTHOR INFORMATION

Corresponding Authors

Rui Sun – *Department of Chemistry, University of Hawai'i at Manoa, Honolulu, Hawaii 96822, United States;* orcid.org/0000-0003-0638-1353; Email: ruisun@hawaii.edu

Ralf I. Kaiser – *Department of Chemistry, University of Hawai'i at Manoa, Honolulu, Hawaii 96822, United States;* orcid.org/0000-0002-7233-7206; Email: ralfk@hawaii.edu

Authors

Koushik Mondal – *Department of Chemistry, University of Hawai'i at Manoa, Honolulu, Hawaii 96822, United States;* orcid.org/0000-0001-7395-4989

Mason McAnally – *Department of Chemistry, University of Hawai'i at Manoa, Honolulu, Hawaii 96822, United States;* orcid.org/0009-0000-7799-9914

Nils Melbourne – *Department of Chemistry, University of Hawai'i at Manoa, Honolulu, Hawaii 96822, United States;* orcid.org/0000-0003-0495-6790

Andrew M. Turner – *Department of Chemistry, University of Hawai'i at Manoa, Honolulu, Hawaii 96822, United States*

Alexandre Bergantini – *Department of Chemistry, University of Hawai'i at Manoa, Honolulu, Hawaii 96822, United States;* Present Address: Centro Federal de Educacao Tecnologica Celso Suckow da Fonseca-CEFET-RJ, Av. Maracana 229, 20271–110 Rio de Janeiro, Brazil; orcid.org/0000-0003-2279-166X

Complete contact information is available at:

https://doi.org/10.1021/acs.jpca.6c02265
J. Phys. Chem. A 2026, 130, 5707–5717

https://pubs.acs.org/10.1021/acs.jpca.6c02265

Notes

The authors declare no competing financial interest.

■ ACKNOWLEDGMENTS

This study was funded through the NSF award, 2330175, Center: NSF Engineering Research Center for Environmentally Applied Refrigerant Technology Hub.

■ REFERENCES

(1) Abbatt, J. P. D.; Thomas, J. L.; Abrahamsson, K.; Boxe, C.; Granfors, A.; Jones, A. E.; King, M. D.; Saiz-Lopez, A.; Shepson, P. B.; Sodeau, J.; et al. Halogen Activation via Interactions with Environmental Ice and Snow in the Polar Lower Troposphere and Other Regions. *Atmos. Chem. Phys.* **2012**, *12*, 6237−6271.

(2) Bartels-Rausch, T.; Jacobi, H.-W.; Kahan, T. F.; Thomas, J. L.; Thomson, E. S.; Abbatt, J. P. D.; Ammann, M.; Blackford, J. R.; Bluhm, H.; Boxe, C.; Domine, F.; Frey, M. M.; Gladich, I.; Guzmán, M. I.; Heger, D.; Huthwelker, Th.; Klán, P.; Kuhs, W. F.; Kuo, M. H.; Maus, S.; Moussa, S. G.; McNeill, V. F.; Newberg, J. T.; Pettersson, J. B. C.; Roeselová, M.; Sodeau, J. R. A review of air−ice chemical and physical interactions (AICI): liquids, quasi-liquids, and solids in snow. *Atmos. Chem. Phys.* **2014**, *14*, 1587−1633.

(3) Bartels-Rausch, T.; Creamean, J.; Thomas, J. L.; Willis, M.; Zieger, P. Ten Crucial Unknowns in Atmospheric Chemistry in the Cold. *Faraday Discuss.* **2025**, *258*, 10−22.

(4) Solomon, S. Stratospheric Ozone Depletion: A Review of Concepts and History. *Rev. Geophys.* **1999**, *37*, 275−316.

(5) Hurwitz, M. M.; Fleming, E. L.; Newman, P. A.; Li, F.; Mlawer, E. J.; Cady-Pereira, K.; Bailey, R. Ozone Depletion by Hydrofluorocarbons. *Geophys. Res. Lett.* **2015**, *42*, 8686−8692.

(6) Li, Y.; Zhu, L.; Li, J.; Chen, Y.; Western, L. M.; Young, D.; Mühle, J.; Weiss, R. F.; Krummel, P. B.; Lunder, C. R. Developing the Chemistry Module for 27 Fluorinated Greenhouse Gases: Reactions, Emissions, and Implementation in GEOS-Chem. *Atmos. Environ.* **2025**, *363*, No. 121604.

(7) Vincent, A.; Fujioka, K.; Luo, Y.; Kaiser, R.; Sun, R. Trifluoroacetic acid formation from HFC-134a under atmospheric conditions. *Phys. Chem. Chem. Phys.* **2026**, *28* (7), 4433−4444.

(8) Franklin, J. The atmospheric degradation and impact of 1,1,1,2-tetrafluoroethane (hydrofluorocarbon 134a). *Chemosphere* **1993**, *27* (8), 1565−1601.

(9) Buch, V.; Devlin, J. P. Spectra of Dangling OH Groups on Ice Surfaces. *J. Chem. Phys.* **1991**, *94*, 4091−4092.

(10) Devlin, J. P.; Buch, V. Surface Vibrational Spectroscopy of Water Ice. *J. Phys. Chem. A* **1995**, *99*, 16534−16548.

(11) Rowland, B.; Devlin, J. P. Spectra of Dangling OH Groups at Ice Cluster Surfaces and within Pores of Amorphous Ice. *J. Chem. Phys.* **1991**, *94*, 812−813.

(12) Graham, A. P.; Menzel, A.; Toennies, J. P. Adsorption of Fluoroform on Ice I_h(0001): Structure and Vibrations. *J. Chem. Phys.* **1999**, *111*, 1169−1174.

(13) Holmes, N. S.; Sodeau, J. R. Infrared Spectroscopic Studies of Halocarbon Adsorption on Amorphous Ice. *J. Phys. Chem. A* **1999**, *103*, 467−475.

(14) Jedlovszky, P.; Picaud, S.; Sumi, I. Dependence of the Adsorption of Halogenated Methane Derivatives at the Ice Surface on Their Chemical Structure. *J. Mol. Liq.* **2017**, *245*, 17−26.

(15) Moreno, E.; Aranda, A.; Díaz-de-Mera, Y.; Martínez, E.; Bravo, I.; Rodríguez, A. The Role of Tropospheric Ice Surfaces in the Elimination of the CFC Substitute Trifluoroethanol. *Phys. Chem. Chem. Phys.* **2012**, *14*, 4425−4432.

(16) Sumi, I.; Fábián, B.; Picaud, S.; Jedlovszky, P. Adsorption of Fluorinated Methane Derivatives at the Surface of Ice under Tropospheric Conditions. *J. Phys. Chem. C* **2016**, *120*, 17386−17399.

(17) Arp, H. P. H.; Gredelj, A.; Glüge, J.; Scheringer, M.; Cousins, I. T. The Global Threat from the Irreversible Accumulation of Trifluoroacetic Acid (TFA). *Environ. Sci. Technol.* **2024**, *58* (45), 19925−19935.

(18) Biswas, S.; Paul, D.; Mondal, K.; Kaiser, R. I. Simulating atmospheric freezing of single aqueous droplets to ice in a cryogenically cooled ultrasonic levitator. *Proc. Natl. Acad. Sci. U.S.A.* **2025**, *122* (6), No. e2425543122.

(19) Mondal, K.; Biswas, S.; Melbourne, N.; Sun, R.; Kaiser, R. I. Probing the freezing chemistry of singly levitated aqueous trifluoroacetic acid droplets in a cryogenically cooled simulation chamber relevant to Earth's upper troposphere. *Chem. Sci.* **2025**, *16*, 11039−11048.

(20) Turner, A. M.; Abplanalp, M. J.; Kaiser, R. I. Probing the carbon−phosphorus bond coupling in low-temperature phosphine (PH_3)−methane (CH_4) interstellar ice analogues. *Astrophys. J.* **2016**, *819* (2), No. 97.

(21) McAnally, M.; Bocková, J.; Turner, A. M.; Hara, N.; Mikhnova, D.; Meinert, C.; Kaiser, R. I. Abiotic origin of the citric acid cycle intermediates. *Proc. Natl. Acad. Sci. U.S.A.* **2025**, *122* (17), No. e2501839122.

(22) Zhu, C.; Turner, A. M.; Abplanalp, M. J.; Kaiser, R. I.; Webb, B.; Siuzdak, G.; Fortenberry, R. C. An interstellar synthesis of glycerol phosphates. *Astrophys. J. Lett.* **2020**, *899* (1), No. L3.

(23) Turner, A. M.; Abplanalp, M. J.; Bergantini, A.; Frigge, R.; Zhu, C.; Sun, B.-J.; Hsiao, C.-T.; Chang, A. H.; Meinert, C.; Kaiser, R. I. Origin of alkylphosphonic acids in the interstellar medium. *Sci. Adv.* **2019**, *5* (8), No. eaaw4307.

(24) Turner, A. M.; Bergantini, A.; Abplanalp, M. J.; Zhu, C.; Góbi, S.; Sun, B.-J.; Chao, K.-H.; Chang, A. H.; Meinert, C.; Kaiser, R. I. An interstellar synthesis of phosphorus oxoacids. *Nat. Commun.* **2018**, *9* (1), No. 3851.

(25) Mondal, K.; McAnally, M.; Biswas, S.; Melbourne, N. W.; Turner, A. M.; Bergantini, A.; Sun, R.; Kaiser, R. I. Refractive Indices and Infrared Band Strengths of Amorphous Ices of Key Fluorinated Refrigerants 1,1,1,2-Tetrafluoroethane, 2,3,3,3-Tetrafluoropropene, and 3,3,3-Trifluoropropene. *ChemPhysChem* **2026**, *27* (4), No. e202500680.

(26) Beltrán, M.; Molina, R. L.; Aznar, M. Á. S.; Moltó, C. S.; Verdú, C. M. Double Laser for Depth Measurement of Thin Films of Ice. *Sensors* **2015**, *15* (10), 25123−25138.

(27) Collings, M. P.; Dever, J. W.; Fraser, H. J.; McCoustra, M. R. S. Laboratory studies of the interaction of carbon monoxide with water ice. *Astrophys. Space Sci.* **2003**, *285* (3), 633−659.

(28) Doronin, M.; Bertin, M.; Michaut, X.; Philippe, L.; Fillion, J. H. Adsorption energies and prefactor determination for CH_3OH adsorption on graphite. *J. Chem. Phys.* **2015**, *143* (8), No. 084703.

(29) Fayolle, E. C.; Balfe, J.; Loomis, R.; Bergner, J.; Graninger, D.; Rajappan, M.; Öberg, K. I. N_2 and CO Desorption Energies from Water Ice. *Astrophys. J. Lett.* **2016**, *816* (2), No. L28, DOI: 10.3847/2041-8205/816/2/L28.

(30) Minissale, M.; Aikawa, Y.; Bergin, E.; Bertin, M.; Brown, W. A.; Cazaux, S.; Charnley, S. B.; Coutens, A.; Cuppen, H. M.; Guzman, V.; Linnartz, H.; McCoustra, M. R. S.; Rimola, A.; Schrauwen, J. G. M.; Toubin, C.; Ugliengo, P.; Watanabe, N.; Wakelam, V.; Dulieu, F. Thermal Desorption of Interstellar Ices: A Review on the Controlling Parameters and Their Implications from Snowlines to Chemical Complexity. *ACS Earth Space Chem.* **2022**, *6* (3), 597−630.

(31) Redhead, P. A. Thermal desorption of gases. *Vacuum* **1962**, *12* (4), 203−211.

(32) King, D. A. Thermal desorption from metal surfaces: A review. *Surf. Sci.* **1975**, *47* (1), 384−402.

(33) Green, S. D.; Bolina, A. S.; Chen, R.; Collings, M. P.; Brown, W. A.; McCoustra, M. R. S. Applying laboratory thermal desorption data in an interstellar context: sublimation of methanol thin films. *Mon. Not. R. Astron. Soc.* **2009**, *398* (1), 357−367.

(34) Aprà, E.; Bylaska, E. J.; De Jong, W. A.; Govind, N.; Kowalski, K.; Straatsma, T. P.; Valiev, M.; van Dam, H. J.; Alexeev, Y.; Anchell,

J.; et al. NWChem: Past, present, and future. *J. Chem. Phys.* **2020**, *152* (18), No. 184102, DOI: 10.1063/5.0004997.
(35) Spitznagel, G. W.; Clark, T.; Chandrasekhar, J.; Schleyer, P. V. R. Stabilization of methyl anions by first-row substituents. The superiority of diffuse function-augmented basis sets for anion calculations. *J. Comput. Chem.* **1982**, *3* (3), 363−371.
(36) Wong, M. W. Vibrational frequency prediction using density functional theory. *Chem. Phys. Lett.* **1996**, *256* (4−5), 391−399.
(37) Santos, J. C.; Piacentino, E. L.; Bergner, J. B.; Rajappan, M.; Öberg, K. I. H_2S ice sublimation dynamics. *Astron. Astrophys.* **2025**, *698*, No. A254, DOI: 10.1051/0004-6361/202554068.
(38) Hasegawa, T.; Yanagisawa, H.; Nagasawa, T.; Sato, R.; Numadate, N.; Hama, T. Infrared Band Strengths of Dangling OH Features in Amorphous Water at 20 K. *Astrophys. J.* **2024**, *969* (2), No. 134, DOI: 10.3847/1538-4357/ad5318.
(39) Hama, T.; Kuwahata, K.; Watanabe, N.; Kouchi, A.; Kimura, Y.; Chigai, T.; Pirronello, V. The Mechanism of Surface Diffusion of H and D Atoms on Amorphous Solid Water: Existence of Various Potential Sites. *Astrophys. J.* **2012**, *757* (2), No. 185, DOI: 10.1088/0004-637X/757/2/185.
(40) Wang, J.; Marks, J. H.; Inada, S.; Kaiser, R. I. Bottom-up Formation of Phenol (C_6H_5OH) in Interstellar Analog Ices of Acetylene and Water Exposed to Ionizing Radiation. *Astrophys. J.* **2026**, *1000* (1), No. 76.
(41) Biswas, S.; Paul, D.; Mondal, K.; Kaiser, R. I. Simulating atmospheric freezing of single aqueous droplets to Ice in a cryogenically cooled ultrasonic levitator. *Proc. Natl. Acad. Sci. U.S.A.* **2025**, *122* (6), No. e2425543122.
(42) Zheng, W.; Jewitt, D.; Kaiser, R. I. Formation of Hydrogen, Oxygen, and Hydrogen Peroxide in Electron-irradiated Crystalline Water Ice. *Astrophys. J.* **2006**, *639* (1), 534−548.
(43) Bergren, M. S.; Schuh, D.; Sceats, M. G.; Rice, S. A. The OH stretching region infrared spectra of low density amorphous solid water and polycrystalline ice I_h. *J. Chem. Phys.* **1978**, *69* (8), 3477−3482.
(44) Devlin, J. P.; Sadlej, J.; Buch, V. Infrared Spectra of Large H_2O Clusters: New Understanding of the Elusive Bending Mode of Ice. *J. Phys. Chem. A* **2001**, *105* (6), 974−983.
(45) Stevenson, K. P.; Kimmel, G. A.; Dohnálek, Z.; Smith, R. S.; Kay, B. D. Controlling the Morphology of Amorphous Solid Water. *Science* **1999**, *283* (5407), 1505−1507.

https://doi.org/10.1021/acs.jpca.6c02265
J. Phys. Chem. A 2026, 130, 5707−5717